metals

MDPI

Article

Ti-Ta-Cu Biocompatible Alloy System Development via Selective Laser Melting for Prosthetic Applications

Igor Polozov *, Victoria Sokolova, Anna Gracheva, Anton Zolotarev, Victoria Nefyodova and Anatoly Popovich

Institute of Machinery, Materials, and Transport, Peter the Great St. Petersburg Polytechnic University (SPbPU), Polytechnicheskaya, 29, 195251 St. Petersburg, Russia; sokolova_vv@spbstu.ru (V.S.); gracheva_am@spbstu.ru (A.G.); zolotarev_am@spbstu.ru (A.Z.); nefedova_va@spbstu.ru (V.N.); director@immet.spbstu.ru (A.P.)

* Correspondence: polozov_ia@spbstu.ru

Abstract: This study investigated the development of Ti-Ta-Cu alloys via selective laser melting (SLM) for potential prosthetic applications. Ti-Ta-Cu alloys with 10, 15, and 20 wt.% Ta were fabricated using in situ alloying of elemental powders. We examined the effects of Ta content and SLM processing parameters on microstructure, phase composition, mechanical properties, and corrosion resistance. X-ray diffraction analysis revealed an increase in β-phase content with increasing Ta concentration. Microstructural analysis showed a dendritic structure in Ta-rich areas, with remelting strategies improving chemical homogeneity and Ta dissolution. The Ti-20Ta-5Cu alloy exhibited the best balance of strength and ductility, with an ultimate tensile strength of 1011 MPa and elongation of 5.7%. All compositions demonstrated lower elastic moduli (103–109 GPa) compared to traditional titanium alloys. Microhardness values were highest for Ti-15Ta-5Cu, ranging from 359 to 410 $HV_{0.5}$ depending on SLM parameters. Corrosion testing in Hank's solution showed improved pitting resistance for Ti-15Ta-5Cu and Ti-20Ta-5Cu compared to Ti-10Ta-5Cu. The study demonstrates the feasibility of producing Ti-Ta-Cu alloys with tailored properties via SLM, offering potential for customized prosthetic applications with improved biomechanical compatibility and functionality.

Keywords: titanium alloy; biomedical alloys; additive manufacturing; in situ alloying; selective laser melting

Citation: Polozov, I.; Sokolova, V.; Gracheva, A.; Zolotarev, A.; Nefyodova, V.; Popovich, A. Ti-Ta-Cu Biocompatible Alloy System Development via Selective Laser Melting for Prosthetic Applications. *Metals* **2024**, *14*, 1177. https://doi.org/10.3390/met14101177

Academic Editor: Thomas Niendorf

Received: 19 September 2024
Revised: 14 October 2024
Accepted: 15 October 2024
Published: 16 October 2024

1. Introduction

Titanium alloys are of particular interest for medical applications due to their high specific strength, corrosion resistance, and bioinertness [1]. The most widely used alloy is the commercially available Ti-6Al-4V, which has been transferred from traditional technologies and gained widespread use. However, controversy surrounding the safety of similar titanium alloys in terms of the toxicity of alloying elements has prompted new directions and concepts related to the engineering of new medical alloys [2]. Another requirement for new alloys is a combination of characteristics that provide the best possible compliance with bone tissue and reduce the stress shielding effect. The presence of regular stresses on both the bone and the implant necessitates the use of a material with high strength and low rigidity [3,4].

The new generation of alloys, such as Ti-Ta-Cu, belongs to a promising class of bioactive materials that stimulate tissue regeneration and prevent the multiplication of pathogens during the post-operation period and rehabilitation [5]. The combination of Ti, Ta, and Cu provides an optimal balance between the mechanical properties, biocompatibility, and functionality of the prosthetic material [6]. This combination of properties is provided by the following factors:

1. Tantalum, being a β-stabilizer of titanium, allows for a reduction in the elastic modulus of the alloy, bringing it closer to the elastic modulus of bone tissue. This is critical

for reducing the 'stress shielding' effect observed during implant use [7]. Tantalum offers an excellent combination of high biocompatibility and specific strength properties. Its low ion emission and the formation of a passivation film on the surface promote better interaction between the implant and bone tissue, making it suitable for medical materials [8]. In its pure form, tantalum has a high density and cost, and its machinability is complicated by its high melting point (~3000 °C) and the formation of an oxide compound on the surface. Previous studies have demonstrated the possibility of processing both pure Ta and binary systems based on it [9,10]. However, the issue of synthesizing Ti-Ta systems from initial powders in the process of additive manufacturing remains open.

2. Copper, when introduced in small quantities, imparts antibacterial properties to the alloy, which is especially important for decreasing the risk of postoperative infections during prosthetics [8]. A notable regeneration-stimulating effect of copper has been observed, with relative elongation increasing up to 26% when added in quantities up to 10 wt.% to CpTi and Ti6Al4V [11–14]. Copper ions are known to promote angiogenesis and osteogenesis when introduced into Ti-6Al-4V alloy [15]. For instance, Ti3Al2V-2Cu, Ti3Al2V-3Cu, Ti3Al2V-10Ta, and Ti3Al2V-10Ta-3Cu compositions used in LPBF have been prepared and investigated for bacterial resistance (dense) and in vivo biological response studies [6].

Copper alloying is used in titanium alloys to reduce embrittlement and the temperature gradient characteristic of the selective laser melting process, and to promote strength in the binary alloy due to the formation of eutectoid grains [16–18].

The selective laser melting (SLM) technology offers the possibility of creating gradient structures and materials with controlled porosity, which is particularly important for optimizing the osseointegration and mechanical properties of customized medical implants and prostheses [19].

In this study, we applied the SLM process to in situ synthesize Ti-Ta-Cu alloys from a mixture of elemental powders. This approach was chosen due to the following advantages:

1. The ability to precisely control the alloy composition by adjusting the proportions of the starting powders, which allows for optimization of material properties for specific prosthetic applications [20,21].
2. The formation of a unique microstructure due to high heating and cooling rates during the SLM process, which can lead to improved mechanical and functional properties of the alloy [22].

Despite the potential advantages of the Ti-Ta-Cu system and the in situ synthesis method for SLM, research in this area remains limited. Most existing works focus on conventional fabrication methods or simpler two-component systems [16,23]. A comprehensive study of the relationship between SLM parameters, microstructure, and properties of Ti-Ta-Cu alloys is critical for optimizing the fabrication process and expanding the application of these promising materials in prosthetics.

This work presents a systematic study of selective laser melting technology modes and their influence on the microstructure, density, hardness, and mechanical properties of Ti-Ta-Cu alloys with variable tantalum content (10, 15, and 20 wt.%). We aim to determine the dependencies between the laser radiation energy density and scanning strategy and their influence on the formation of the microstructure and properties of the obtained samples. A detailed analysis of the structure formation will extend the understanding of the peculiarities of multi-component titanium alloys additive manufacturing and optimize the processes of obtaining materials with specified properties, optimal for use in prosthetics.

2. Materials and Methods

To investigate the effects of copper in situ alloying on the microstructure and properties of Ti-Ta-Cu alloys, powder mixtures were obtained by mixing Ti and Ta powders in amounts of 10, 15, and 20 wt.% using a gravity mixer. The Ta powder consisted of fragmented particles with a size of 24.6 μm, while the gas-atomized Ti powder had a spherical shape

with a particle size of 36 µm (Figure 1a,b). Elemental copper powder with a dendritic particle shape and a median particle size of 37 µm was added to the Ti-Ta powder mix in a tumbler mixer for 12 h (Figure 1c). Powder mixtures with different copper content were prepared: Ti-10Ta-5Cu, Ti-15Ta-5Cu, and Ti-20Ta-5Cu, corresponding to 10, 15, and 20 wt.% of tantalum, respectively.

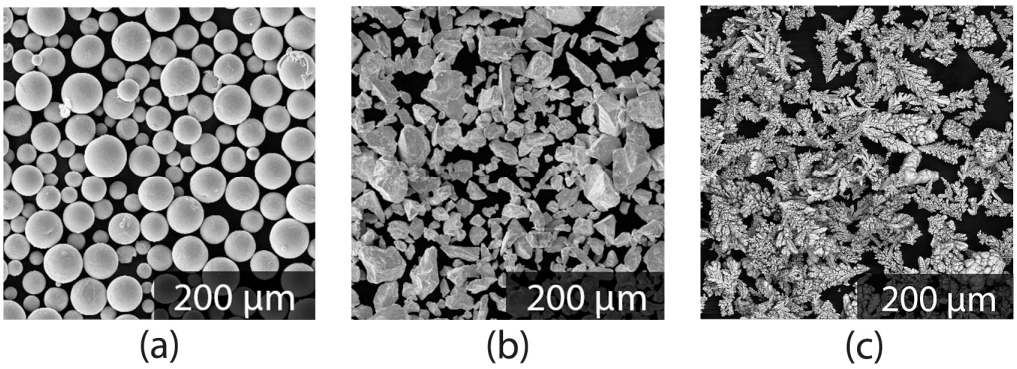

Figure 1. SEM images of initial titanium (**a**) tantalum (**b**) and copper (**c**) powder.

Cubic samples (10 × 10 × 10 mm) were fabricated from the prepared mixture using the SLM method on a 3DLam Mini (3DLam, St. Petersburg, Russia) machine, fitted with a fiber laser with a maximum power of 300 W, in a protective argon atmosphere. To study the possibility of obtaining Ti-Ta-Cu alloys, various scanning modes were utilized (Table 1): LE—low energy, ME—medium energy, HE—high energy, UHE—ultra high energy, S—single scan, R1—1 time remelting, R2—2 times remelting, D—dense hatch distance.

Table 1. Selective laser melting parameters.

Mode	Power, W	Scanning Speed, mm/s	Hatch Distance, mm	Layer Thickness, mm	Energy Density, J/mm^3	Remelting
LE-S	130	550	0.14	0.03	56	No
ME-S	190	550	0.14	0.03	82	No
HE-S	250	550	0.14	0.03	108	No
ME-R1	220	550	0.14	0.03	95	Yes (1 time)
ME-R2	220	550	0.14	0.03	95	Yes (2 times)
UHE-D	110	400	0.035	0.03	262	Yes (1 time)

The as-printed condition, including the amount of unmelted Ta particles, was quantified via digital image analysis using ImageJ software (version 1.52) and thresholding techniques as described in [24,25]. Polished sections corresponding to the OZ direction of printing were prepared in advance. Density measurements utilized the Archimedes method as outlined in the ASTM B962 standard [26].

Microstructural and energy dispersive analyses (EDX) were conducted using a Mira 3 LMU scanning electron microscope (Tescan, Czech Republic). X-ray diffraction phase analysis (XRD) was performed using a Bruker D8 Advance X-ray diffractometer (Bruker, Bremen, Germany) with CuKα radiation (λ = 1.5418 Å).

Hardness measurements of the samples were taken using a Buehler VH1150 unit (Buehler, Lake Bluff, IL, USA) under a 500 g weight. Tensile tests were conducted on a Zwick/Roell Z100 testing machine (Zwick/Roell, Germany). Cylindrical tensile specimens were prepared according to the ASTM E8/E8M standard [27] for metallic materials, with a gauge length of 25 mm and a diameter of 6.25 mm. The tests were performed at room temperature with a strain rate of 0.001 s^{-1}.

Corrosion resistance was determined in a temperature-controlled open cell using a VersaStat 4 Princeton Applied Research potentiostat (AMETEK, Berwyn, IL, USA). Linear

anodic polarization was employed in a prepared sterile Hank's balanced salt solution (HBSS) with a production pH of 6.8–7.2 at 36.5 ± 0.5 °C. The HBSS composition was as follows (in g/L): 8.00 NaCl, 0.40 KCl, 0.14 $CaCl_2$, 0.06 $MgSO_4 \cdot 7H_2O$, 0.06 $NaH_2PO_4 \cdot 2H_2O$, 0.35 $NaHCO_3$, 1.00 glucose, and 0.06 KH_2PO_4. This solution closely mimics the ion concentrations found in human blood plasma, making it suitable for simulating the corrosive environment that implants may encounter in the human body.

A single-key Ag | AgCl chlorosilver electrode was used as a reference electrode and a platinum laboratory electrode EPL-02 as an auxiliary electrode. The current lead, in the form of a copper wire, was attached to the obtained samples, which were prepared as 20 × 20 × 2 mm plates with a hole for fixing the current lead. The surface of the samples was subjected to grinding using abrasive paper with grit 180–1200 and polishing to 9 microns using polishing cloths on a BUEHLER ECOMET 4 grinding and polishing machine.

The non-tested parts of each specimen were insulated with a lacquer heat-resistant coating so that the tested surface area was 1 cm^2. Prior to testing, the surface of the samples was degreased using an alcohol-containing solution and acetone.

In alignment with the research objectives of identifying critical processing-structure-property relationships, a selective approach was taken in testing SLM modes for different experiments. The modes chosen for each test represent a range of energy densities and processing strategies, enabling the identification of key trends and relationships in the Ti-Ta-Cu alloy system. For density measurements, modes representing extremes in energy input (HE-S and UHE-D) were compared with the baseline mode (ME-S) and a remelting strategy (ME-R1). Microhardness testing included most modes but excluded LE-S due to its poor densification results in preliminary tests. Tensile tests were conducted only for the ME-S mode, which showed the best balance of density and microstructure in initial evaluations. The UHE—D (ultra high energy—dense) mode was specifically designed to investigate the effect of extremely high energy density on the material properties. In this mode, both the scanning speed and hatch distance are significantly reduced compared to other modes. The lower scanning speed allows for a longer laser–material interaction time, while the reduced hatch distance increases the overlap between adjacent scan tracks. Together, these changes result in a much higher energy density input to the material. This extreme condition was included to explore the upper limits of energy input and its effects on the microstructure and properties, particularly for alloys with higher melting point elements like tantalum.

3. Results

3.1. Density Evaluation

The density measurement results of the samples obtained using the SLM method at different regimes are shown in Figure 2 for Ti-10Ta-5Cu, Ti-15Ta-5Cu, and Ti-20Ta-5Cu alloys. The experimental densities of the alloys are presented in Table 2.

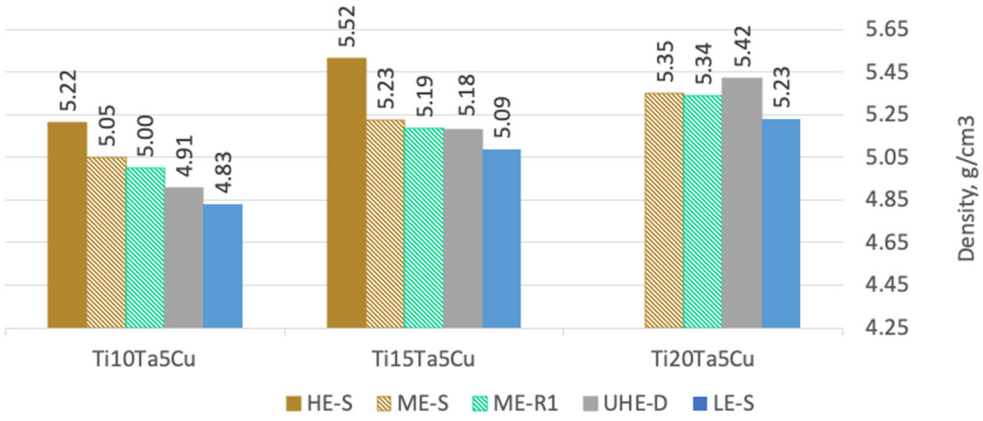

Figure 2. Density dependence of samples on the SLM mode for three alloy compositions.

Table 2. Experimental density of Ti-Ta-Cu alloys.

	Ti-10Ta-5Cu	Ti-15Ta-5Cu	Ti-20Ta-5Cu
Density, g/cm^3	5.02 ± 0.06	5.22 ± 0.12	5.37 ± 0.04

It was observed that the density of the synthesized material increased with an increase in the content of tantalum, which has a relatively high atomic mass. Within the compositions Ti-10Ta-5Cu and Ti-15Ta-5Cu, the HE-S mode, characterized by the highest laser irradiation power, contributed to the highest density of the synthesized alloys. The remelting modes (ME-R1 and ME-R2) showed no significant increase in density compared to single scanning at the same energy (ME-S) for all compositions investigated. However, these modes may be effective in eliminating individual tantalum particles in the alloys.

The low energy density regime (LE-S) resulted in significantly lower density compared to other modes across all compositions. This can be attributed to insufficient energy input to fully melt the powder particles, particularly the high-melting-point tantalum. The lower density in the LE-S mode indicates incomplete fusion and increased porosity, which explains its exclusion from further mechanical testing.

The use of high energy density due to small pass spacing (UHE-D mode) led to higher densities in Ti-20Ta-5Cu but resulted in the lowest density in Ti-10Ta-5Cu. The UHE-D mode proved to be the most effective for the melting of tight-melting tantalum but was found to be redundant for obtaining Ti-10Ta-5Cu alloy with a lower Ta content, causing the transition of powder mixture components during high-temperature laser exposure to the gaseous phase and resulting in a high porosity of the material.

The effect of energy density on the final density of the samples was not linear and depended on the alloy composition. For Ti-10Ta-5Cu and Ti-20Ta-5Cu, there was a tendency for the density to increase with increasing energy density, while for Ti-15Ta-5Cu this dependence was not as unambiguous.

3.2. Microstructure

The microstructure of samples obtained as a result of selective laser melting was generally observed to be a non-homogeneous material with the presence of unmelted Ta particles and the absence of pronounced grains (Figure 3a). Under significant magnification, the microstructure of as-SLMed Ti-Ta-5Cu was generally represented by a mixture of tantalum-enriched areas and titanium-enriched areas (light areas—tantalum, dark areas—titanium). The selected printing parameters did not provide sufficient mixing of the elements in the melt bath, and therefore, liquation areas repeating their shape were observed in the OZ direction (Figure 3b). Tantalum-enriched areas exhibited a dendritic structure typical for Cu-containing titanium alloys.

Figure 4 illustrates the microstructure of as-SLMed Ti-Ta-Cu alloys under different processing conditions. The ME-S mode for Ti-10Ta-5Cu (Figure 4a) and Ti-20Ta-5Cu (Figure 4c) showed distinct differences in tantalum distribution. The remelting ME-R1 and ME-R2 modes were found to be effective strategies for chemical homogenization and dissolution of tantalum powder. In particular, the ME-R2 mode (Figure 4b,d) promoted a three times lower Ta particle content in the alloy compared to the single scan mode.

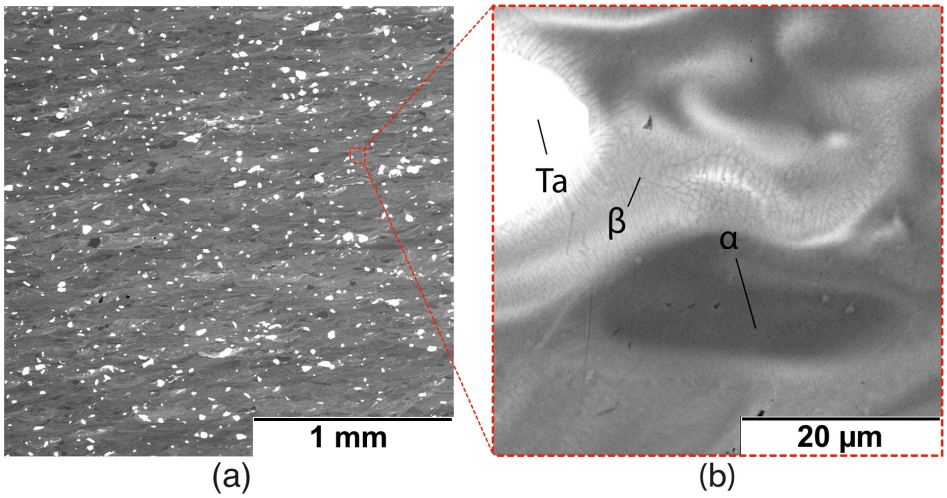

Figure 3. Microstructure of as-SLMed Ti15Ta5Cu alloy at different magnifications: (**a**) general view of the microstructure, (**b**) microstructure at a higher magnification.

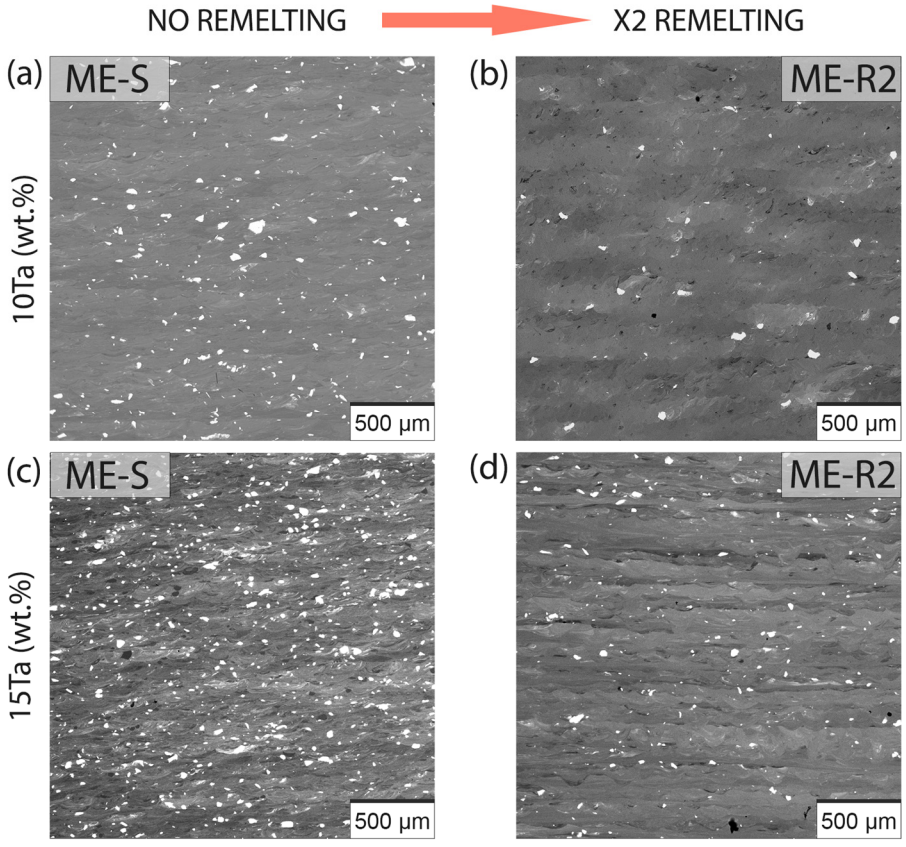

Figure 4. Microstructure of as-SLMed Ti-Ta-Cu alloys: (**a**) ME-S mode for Ti10Ta5Cu, (**b**) ME-R2 mode for Ti15Ta5Cu, (**c**) ME-S mode for Ti10Ta5Cu, (**d**) ME-R2 mode for Ti15Ta5Cu.

3.3. Phase Composition

Figure 5 shows the XRD patterns of Ti-Ta-Cu alloys with different Ta content. XRD evaluation revealed the presence of main α-Ti (JCPDS file #44-1294) and β-phase (JCPDS file #44-1288), with no obvious diffraction peaks of any copper-based eutectoid at 5 wt.% Cu content. According to the phase diagram, the β-phase may be present as a Ti-Ta-Cu solid solution. Different phase states were observed during the application of scanning strategies with multiple remelting (ME-R1, ME-R2).

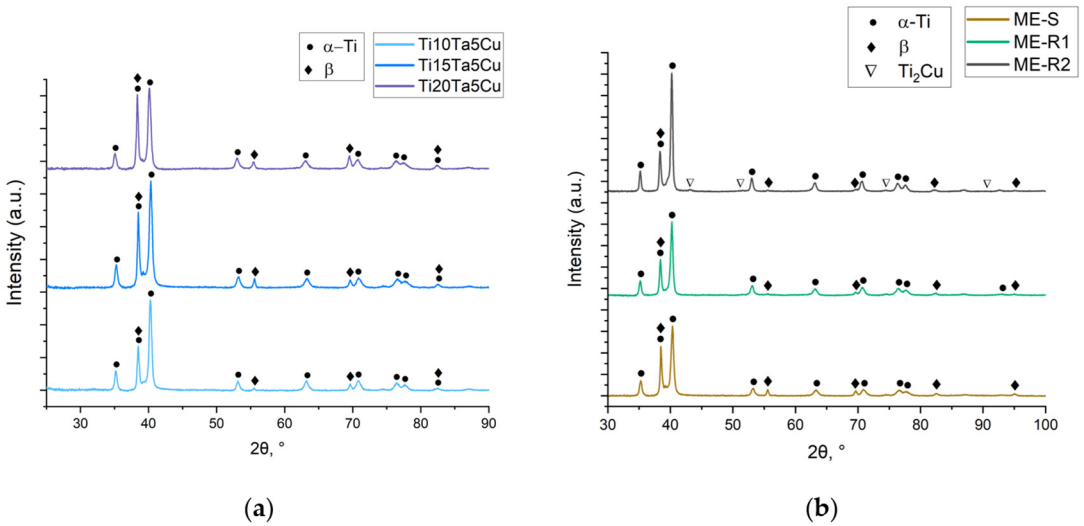

(**a**) (**b**)

Figure 5. XRD diffractograms of Ti-Ta-Cu samples: (**a**) with various Ta content (wt.%), (**b**) Ti-15Ta-5Cu at different SLM modes.

As shown in Figure 5, with an increasing number of remelting passes (ME-R2), the phase composition changed. The intensity of beta-phase peaks decreased, and Cu-based intermetallic compound Ti_2Cu peaks (JCPDS file #18-0468) were identified, which is characteristic of titanium alloys in the presence of copper [23]. The amount of formed Ti_2Cu did not appear to depend on the change of Ta content in the alloy. However, cyclic heating and cooling at high rates during remelting treatment (ME-R1, ME-R2) led to destabilization and decomposition of β-phase with the formation of α-Ti and eutectoid Ti_2Cu. Under non-equilibrium conditions due to the high cooling rate of the melt during laser treatment (about 10^5 K/s), the formation of Ti_2Cu was observed to be slowed down, despite the high diffusion activity of copper [23,28].

Stabilization of beta-phase due to the increase in tantalum content was confirmed via the results of XRD analysis (Figure 5). XRD analysis showed an increase of the β-phase peaks characterizing the solid solution (Ti, Ta, Cu) under the conditions of one scanning mode, with no intermetallic compounds with copper detected.

3.4. Chemical Composition

The chemical composition was analyzed via energy dispersive X-ray spectroscopy (EDX). The results are presented in Table 3. EDX spectra for Ti-10Ta-5Cu, Ti-15Ta-5Cu, and Ti-20Ta-5Cu samples obtained under the ME-S regime showed that the actual chemical composition of the samples was close to the nominal composition of the initial powder mixture.

Table 3. Chemical composition of samples obtained under ME-S mode (wt.%).

	Ti-10Ta-5Cu	**Ti-15Ta-5Cu**	**Ti-20Ta-5Cu**
Ti	85.2 ± 0.8	80.3 ± 0.7	75.4 ± 0.9
Ta	9.8 ± 0.5	14.7 ± 0.6	19.6 ± 0.7
Cu	5.0 ± 0.3	5.0 ± 0.3	5.0 ± 0.3

A slight deviation of tantalum content from the nominal value (by 0.2–0.4 wt.%) was observed, which could be associated with a different distribution of powder in the sample volume. Nevertheless, despite the large difference in the melting temperatures of the components under normal conditions (Ti—1668 °C, Ta—3020 °C, Cu—1085 °C), vaporization of elements such as Ti and Cu after the high-energy SLM processing was not detected.

3.5. Electrochemical Characterization

To evaluate the corrosion behavior of the Ti-Ta-Cu alloys, open circuit potential (OCP) measurements and potentiodynamic polarization tests were conducted in Hank's balanced salt solution at 36.5 ± 0.5 °C. Figure 6 shows the OCP curves and potentiodynamic polarization curves for the Ti-10Ta-5Cu, Ti-15Ta-5Cu, and Ti-20Ta-5Cu alloys.

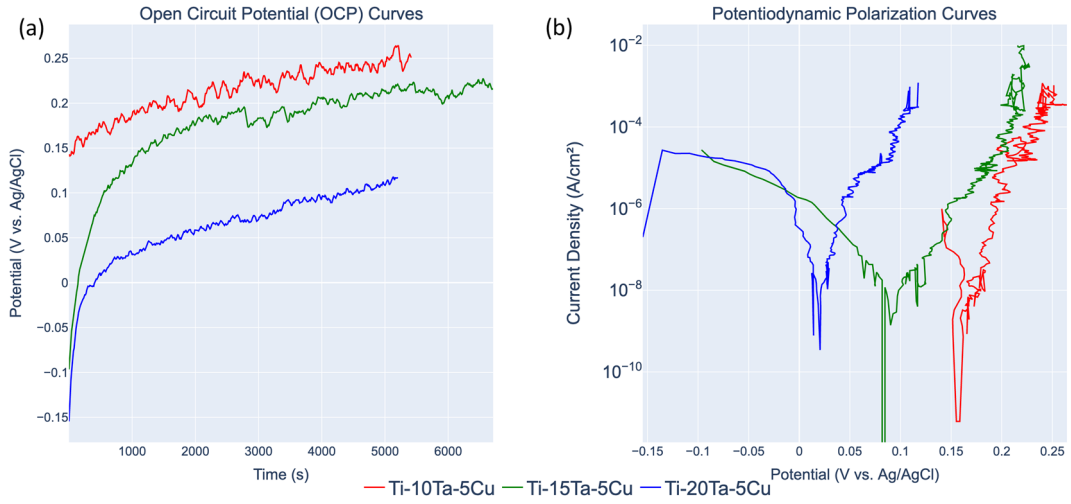

Figure 6. Electrochemical characterization of Ti-Ta-Cu alloys in Hank's solution at 36.5 ± 0.5 °C: (**a**) open circuit potential (OCP) curves and (**b**) potentiodynamic polarization curves.

The OCP curves (Figure 6a) reveal the evolution of the open circuit potential over time for the three alloy compositions. All alloys exhibit a gradual increase in potential, indicating the formation and growth of a passive oxide layer on the surface. The Ti-10Ta-5Cu alloy shows the most noble initial potential, while Ti-20Ta-5Cu starts from the most active potential. By the end of the 5-h measurement period, the potentials for all alloys stabilize, with Ti-15Ta-5Cu and Ti-20Ta-5Cu converging to similar values, slightly nobler than Ti-10Ta-5Cu.

Figure 6b presents the potentiodynamic polarization curves for the three alloy compositions. These curves demonstrate that all three alloys exhibit passive behavior over a wide potential range, indicated by the relatively stable current density over a range of potentials. The Ti-15Ta-5Cu and Ti-20Ta-5Cu alloys show wider passive regions compared to Ti-10Ta-5Cu, suggesting superior corrosion resistance. The Ti-20Ta-5Cu alloy displays the lowest corrosion current density, indicating the highest resistance to uniform corrosion among the three compositions.

Table 4 summarizes the key electrochemical parameters extracted from these curves, including the corrosion potential, E_{corr}, pitting potential, E_{pit}, and corrosion current density, i_{corr}. Corrosion potentials, E_{corr}, and pitting potentials, E_{pit}, were determined from the obtained curves via a graphical method. The base of pitting resistance was determined as the difference of pitting formation potential and corrosion potential. The corrosion current densities, i_{corr}, were determined using the Tafel extrapolation method. The Ti-20Ta-5Cu alloy exhibited the lowest i_{corr} value of 0.038 μA/cm^2, confirming its superior corrosion resistance. This is consistent with its more noble E_{corr} and wide passive region observed in the potentiodynamic curve.

Table 4. Results of electrochemical characterization for different Ti-Ta-Cu composition.

	E_{OC}, V	E_{corr}, V	E_{pit}, V	i_{corr}, μA/cm^2
Ti-10Ta-5Cu	0.36	−0.1	3.53	0.052
Ti-15Ta-5Cu	0.23	−0.1	4.13	0.045
Ti-20Ta-5Cu	0.26	−0.01	3.62	0.038

According to the results of electrochemical characterization (Table 4), the Ti-10Ta-5Cu sample exhibited the lowest resistance to corrosion compared to alloys with 15 and 20 wt% Ta, whose potentials were 0.23 V and 0.26 V, respectively. The results of electrochemical investigations of titanium alloys with different tantalum content showed that the highest resistance to pitting corrosion in the given model solution was demonstrated by samples of Ti-15Ta-5Cu alloy, whose pitting resistance basis was 4.13 V. The study of Ti-20Ta-5Cu showed slight deterioration of pitting resistance compared to Ti-15Ta-5Cu, which was associated with an increase in pitting centers—unmelted Ta particles and with the development of corrosion anodic-cathodic processes at the interface between Ti and Ta.

3.6. Microhardness

The microhardness measurement results of Ti-Ta-Cu samples are shown in Figure 7.

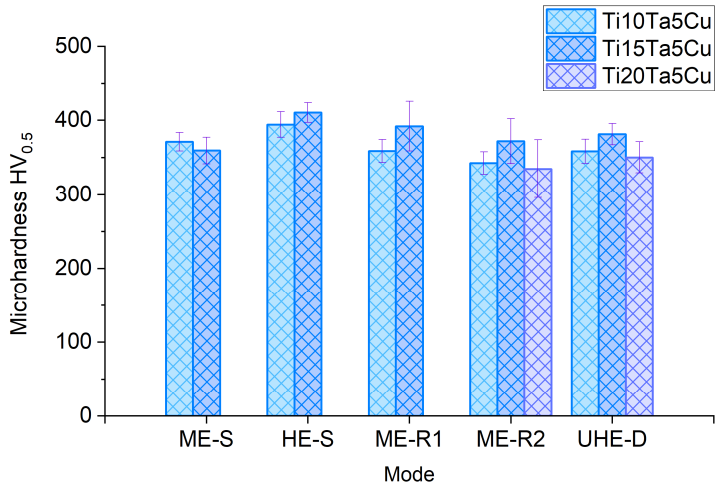

Figure 7. Microhardnesses of Ti-xTa-5Cu samples with various Ta (wt.%) content at different SLM scanning modes.

With increasing tantalum content, no significant microhardness increase was observed. The highest microhardness values were observed in the Ti-Ta-Cu alloy with 15 wt.% Ta, independent of the SLM scanning strategy, with the highest value reaching 391.80 ± 33.24 $HV_{0.5}$.

High energy density regimes (HE-S and UHE-D) led to a slight decrease in microhardness compared to medium energy regimes, which may be attributed to the formation of a coarser grain structure. The remelting scanning strategies (ME-R1 and ME-R2) showed a tendency for lower microhardness, which could be due to the formation of a more homogeneous structure and reduced porosity.

The microhardness values for the Ti-15Ta-5Cu alloy ranged from 359 to 410 $HV_{0.5}$, depending on the SLM parameters used. This variability in microhardness demonstrates the significant influence of processing parameters on the mechanical properties of the alloy.

For the Ti-10Ta-5Cu and Ti-20Ta-5Cu alloys, the microhardness values were generally lower than those of Ti-15Ta-5Cu across all scanning modes. This trend suggests that the 15 wt.% Ta composition may provide an optimal balance of phases and microstructure for enhanced hardness in this alloy system.

3.7. Mechanical Characterization

The values of tensile strength, yield strength, and elongation for each alloy tested are summarized in Table 5 and Figure 8.

Table 5. Tensile mechanical properties of samples obtained under ME-S mode.

Composition	Mode	E, GPa	Yield Strength, MPa	Ultimate Tensile Strength, MPa	Elongation at Break, %
Ti-10Ta-5Cu	ME-S	103	-	1260	-
Ti-15Ta-5Cu	ME-S	109	1310	1435	0.4
Ti-20Ta-5Cu	ME-S	107	899	1011	5.7

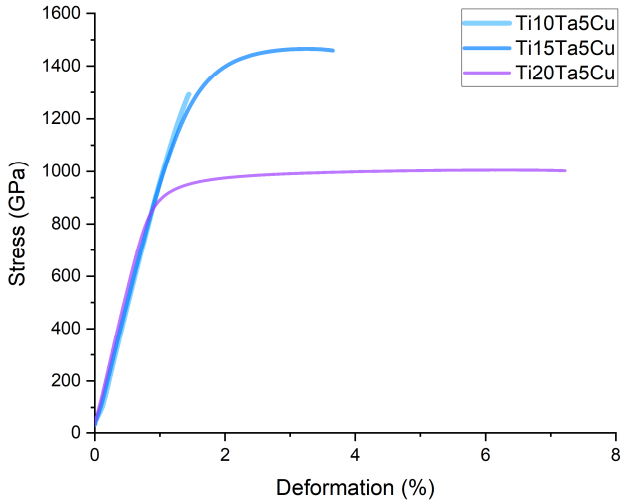

Figure 8. Tensile diagrams for Ti-10Ta-5Cu, Ti-15Ta-5Cu, and Ti-20Ta-5Cu samples after SLM processing with ME-S scanning mode.

According to Figure 7, an increase in Ta content was observed to significantly affect the plastic deformation of the as-SLMed alloy. The Ti-10Ta-5Cu alloy exhibited brittle fracture without measurable plastic deformation; hence, no data on yield strength and relative elongation were available for this composition.

The Ti-15Ta-5Cu alloy demonstrated the highest ultimate tensile strength of 1435 MPa but showed low ductility with only 0.4% elongation. In contrast, the Ti-20Ta-5Cu alloy exhibited the best balance of strength and ductility, with an ultimate tensile strength of 1011 MPa and an elongation at break of 5.7%. This improved ductility in the Ti-20Ta-5Cu alloy may be attributed to the optimal ratio of α- and β-phases in its microstructure.

The modulus of elasticity (E) of all investigated compositions was found to be in the range of 103–109 GPa. These values are lower than those of traditional titanium alloys (e.g., Ti-6Al-4V with E ≈ 110–120 GPa), which is considered favorable for prosthetic applications [29]. The lower elastic modulus can potentially reduce the stress shielding effects in implants, leading to better biomechanical compatibility.

4. Discussion

4.1. Influence of Alloy Composition on Structure and Properties

The analysis of the obtained results shows that the tantalum content in the alloys of the Ti-Ta-Cu system has a significant effect on their structure and properties:

1. An increase of tantalum content from 10 to 20 weight % led to an increase of alloy density from 5.02 to 5.37 g/cm^3. This can be attributed to the higher atomic mass of tantalum compared to titanium and is in accordance with the rule of mixtures. A similar trend was observed in Zhou et al. [30] for Ti-Ta alloys produced via casting.
2. X-ray diffraction analysis revealed an increase in the proportion of β-phase in the alloy structure with increasing tantalum content. Such β-stabilizing effect of tantalum, also observed in the studies by Liu et al. [31], could be an effective medium for Ti_2Cu precipitates suppression. The presence of Ta was found to refine the grain in Ta-rich areas, forming a dendrite-like microstructure.

3. The microhardness of the alloys decreased with increasing tantalum content, which can be explained by a combination of solid-solution hardening and an increase in the proportion of the β-phase.
4. Tensile mechanical properties showed that the Ti-20Ta-5Cu alloy had the best balance of strength and ductility. This may be due to the optimal ratio of α- and β-phases as well as a more homogeneous microstructure. A similar optimization of mechanical properties by controlling the phase composition was observed in the study of Zhenhuan et al. [32] for Ti-Ta-Nb-Zr alloy.

4.2. Influence of SLM Modes on Structure and Properties

The application of different scanning modes within the same alloy showed that the Ti-10Ta-Cu alloy was the most sensitive to changes in energy density due to variations in laser power. The scanning strategy with the lowest energy density (ME-S) proved to be the most suitable for obtaining the most defect-free material, despite the largest amount of undissolved Ta in the alloy. Multiple scans (ME-R1 mode) were effective in eliminating this disadvantage.

The scanning strategy with the highest energy density (UHE-D) led to the formation of gas pores in Ti-10Ta-Cu but was beneficial when the Ta content increased up to 20 wt.%. For Ti-20Ta-5Cu, the effect of energy density was less pronounced, which may indicate a wider process window for this composition. This could be attributed to the change in the thermophysical properties of the alloy with increasing tantalum content, such as the thermal conductivity and melting point.

The modes with high energy density (HE-S and UHE-D) provided the highest density of the samples, which is associated with more complete melting of the powder and a reduction of porosity. This observation aligns with findings by Kasperovich and Hausmann [33], who reported similar effects of energy density on porosity in Ti-6Al-4V alloys processed via SLM.

The Ti-15Ta-Cu alloy showed the most stable density values across the considered modes (ME-S, ME-R1, UHE-D), except for a maximum at the HE-S regime. This behavior may be due to the optimal balance between the completeness of melting and minimizing the formation of defects, such as pores and cracks, which can occur at excess energy input [34].

The use of remelting (modes ME-R1 and ME-R2) contributed to an increase in chemical and structural homogeneity due to 30% better Ta dissolution and a decrease in the number of defects. However, these modes provided the formation of a coarser grain structure, which can negatively affect mechanical properties. This trade-off between homogeneity and grain size is consistent with observations by Thijs et al. [35] in their study of SLM-processed Ti-6Al-4V.

The low energy density regime led to the formation of a more porous structure and, consequently, to a decrease in the density and mechanical properties of the samples. This relationship between energy density and porosity in titanium alloys obtained using the SLM method has been well-documented in previous studies [36].

4.3. Effect of SLM Modes on Chemical Composition

High energy density regimes (HE-S and UHE-D) showed a slight (up to 0.3 wt.%) decrease in Cu content compared to the nominal composition, which may be attributed to partial vaporization of Cu at higher process temperatures.

The modes with repeated remelting (ME-R1 and ME-R2) did not lead to a significant change in the chemical composition compared to the single-scanning mode (ME-S), which indicates the stability of the composition under repeated exposure to laser radiation. This compositional stability is crucial for maintaining consistent properties throughout the fabricated parts and suggests that these remelting strategies can be employed to improve homogeneity without compromising the intended alloy composition.

The results confirm the efficiency of the in situ method for the synthesis of Ti-Ta-Cu alloys via selective laser melting and demonstrate the possibility of precise control of

the chemical composition of the obtained materials. This level of compositional control is particularly important for biomedical applications, where slight variations in alloy chemistry can significantly impact the biocompatibility and mechanical performance.

The observed stability of Ti and Ta contents across different SLM modes, despite their significantly different melting points, highlights the robustness of the SLM process for processing multi-component alloys. This stability is advantageous for producing components with consistent properties throughout complex geometries, which is often challenging in conventional manufacturing methods.

The slight variations in Ta content (0.2–0.4 wt.%) observed across different samples may be attributed to the inhomogeneous distribution of powder in the initial mixture rather than process-induced compositional changes. This underscores the importance of powder mixing techniques in achieving consistent compositions in SLM-processed multi-component alloys.

4.4. Prospects for Ti-Ta-Cu Alloys Application for Prosthetics

Based on the results obtained, the following conclusions can be drawn about the prospects for the application of the studied alloys in prosthetics:

1. All investigated compositions demonstrated lower modulus of elasticity (103–109 GPa) in comparison with traditional titanium alloys, which is favorable for reducing the effect of "stress shielding" in implants. This is in agreement with the work of Niinomi et al. [37], which emphasizes the importance of lowering the elastic modulus to improve the biomechanical compatibility of implants.
2. Ti-20Ta-5Cu alloy showed the best balance of strength and ductility, which makes it the most promising for use in loaded prosthetic elements. The ultimate tensile strength of 1011 MPa combined with an elongation at break of 5.7% suggests good mechanical performance under various loading conditions.
3. The high microhardness of the Ti-15Ta-5Cu can provide good wear resistance, which is important for denture durability. This could be particularly beneficial in applications where the prosthetic component is subject to friction and wear.
4. The presence of copper in alloys potentially provides antibacterial properties, which may reduce the risk of postoperative infections. The antibacterial effect of copper in titanium alloys for biomedical applications was demonstrated in a study by Liu et al. [38].
5. The possibility of controlling the structure and properties of alloys by changing the parameters of SLM opens up prospects for creating gradient structures and optimizing the properties of different parts of the prosthesis [39]. This flexibility in manufacturing could allow for the creation of prosthetics with tailored properties in different regions to match the varying mechanical and biological requirements across the implant.

The obtained results demonstrate the promising application of Ti-Ta-Cu system alloys obtained via selective laser melting to create new materials in the field of medical prosthetics. The combination of a lower elastic modulus, good mechanical strength, potential wear resistance, and possible antibacterial properties makes these alloys attractive candidates for further development and testing in biomedical applications.

5. Conclusions

This study demonstrates the successful fabrication of Ti-Ta-Cu alloys via selective laser melting, with compositions tailored for potential prosthetic applications. The key findings are:

1. Increasing the tantalum content from 10 to 20 wt.% led to enhanced β-phase formation, improved chemical homogeneity, and a better balance of strength and ductility.
2. Ti-20Ta-5Cu alloy exhibited the most promising combination of properties, with an ultimate tensile strength of 1011 MPa, 5.7% elongation, and an elastic modulus of 107 GPa.

3. All investigated compositions showed lower elastic moduli (103–109 GPa) compared to traditional titanium alloys, potentially reducing stress shielding in implants.
4. Ti-15Ta-5Cu demonstrated the highest microhardness and best corrosion resistance, with a pitting resistance basis of 4.13 V in Hank's solution.
5. Remelting strategies in SLM processing improved chemical homogeneity and Ta dissolution, enhancing overall alloy performance.

These results indicate that Ti-Ta-Cu alloys, particularly Ti-15Ta-5Cu and Ti-20Ta-5Cu, are promising candidates for biomedical implants, offering improved biomechanical compatibility and potential antibacterial properties due to copper content. Future research should focus on in-depth biocompatibility studies, fatigue behavior, and optimization of SLM parameters for creating gradient structures. Additionally, investigating the long-term stability of these alloys in physiological environments and their osseointegration properties would be crucial for their successful application in prosthetics.

Author Contributions: Conceptualization, I.P.; data curation, A.Z.; formal analysis, V.S. and A.G.; funding acquisition, A.P.; investigation, V.S., A.G., A.Z. and V.N.; methodology, I.P.; project administration, A.P.; supervision, I.P.; visualization, V.S. and A.Z.; writing—original draft, V.S. and V.N.; writing—review and editing, I.P. and A.P. All authors have read and agreed to the published version of the manuscript.

Funding: This research was supported by the Ministry of Science and Higher Education of the Russian Federation (agreement No. 075-15-2024-562).

Data Availability Statement: The data presented in this study are available on request from the corresponding author.

Conflicts of Interest: The authors declare no conflicts of interest.

References

1. Salvador, C.A.F.; Maia, E.L.; Costa, F.H.; Escobar, J.D.; Oliveira, J.P. A compilation of experimental data on the mechanical properties and microstructural features of Ti-alloys. *Sci. Data* **2022**, *9*, 188. [CrossRef] [PubMed]
2. Salvador, C.A.F.; Van Landeghem, H.P.; Antunes, R.A. Selection of Ti Alloys for Bio-Implants: An Application of the Ashby Approach with Conflicting Objectives. *Adv. Eng. Mater.* **2023**, *25*, 2301169. [CrossRef]
3. Fleps, I.; Bahaloo, H.; Zysset, P.K.; Ferguson, S.J.; Pálsson, H.; Helgason, B. Empirical relationships between bone density and ultimate strength: A literature review. *J. Mech. Behav. Biomed. Mater.* **2020**, *110*, 103866. [CrossRef] [PubMed]
4. Geetha, M.; Singh, A.K.; Asokamani, R.; Gogia, A.K. Ti based biomaterials, the ultimate choice for orthopaedic implants—A review. *Prog. Mater. Sci.* **2009**, *54*, 397–425. [CrossRef]
5. Yu, X.; Tang, X.; Gohil, S.V.; Laurencin, C.T. Biomaterials for Bone Regenerative Engineering. *Adv. Healthc. Mater.* **2015**, *4*, 1268–1285. [CrossRef]
6. Bandyopadhyay, A.; Mitra, I.; Ciliveri, S.; Avila, J.D.; Dernell, W.; Goodman, S.B.; Bose, S. Additively manufactured Ti–Ta–Cu alloys for the next-generation load-bearing implants. *Int. J. Extrem. Manuf.* **2023**, *6*, 015503. [CrossRef]
7. Zhou, Y.L.; Niinomi, M.; Akahori, T. Effects of Ta content on Young's modulus and tensile properties of binary Ti–Ta alloys for biomedical applications. *Mater. Sci. Eng. A* **2004**, *371*, 283–290. [CrossRef]
8. Hu, X.; You, D.; Fei, T.; Wu, Y.; Shao, Y.; Xie, Y.; Xu, M.; Hu, Y.; Zhang, J.; Yu, M. The role and application of metal ions in maxillofacial bone defect. *Chem. Eng. J.* **2024**, *493*, 152317. [CrossRef]
9. Zhou, L.B.; Shu, J.G.; Sun, J.S.; Chen, J.; He, J.J.; Li, W.; Huang, W.Y.; Niu, Y.; Yuan, T.C. Effects of tantalum addition on microstructure and properties of titanium alloy fabricated by laser powder bed fusion. *J. Cent. South Univ.* **2021**, *28*, 1111–1128. [CrossRef]
10. Wauthle, R.; Van Der Stok, J.; Yavari, S.A.; Van Humbeeck, J.; Kruth, J.P.; Zadpoor, A.A.; Weinans, H.; Mulier, M.; Schrooten, J. Additively manufactured porous tantalum implants. *Acta Biomater.* **2015**, *14*, 217–225. [CrossRef]
11. Liu, H.; Tang, Y.; Zhang, S.; Liu, H.; Wang, Z.; Li, Y.; Wang, X.; Ren, L.; Yang, K.; Qin, L. Anti-infection mechanism of a novel dental implant made of titanium-copper (TiCu) alloy and its mechanism associated with oral microbiology. *Bioact. Mater.* **2022**, *8*, 381–395. [CrossRef] [PubMed]
12. Zhuang, Y.; Ren, L.; Zhang, S.; Wei, X.; Yang, K.; Dai, K. Antibacterial effect of a copper-containing titanium alloy against implant-associated infection induced by methicillin-resistant Staphylococcus aureus. *Acta Biomater.* **2021**, *119*, 472–484. [CrossRef]
13. Ju, J.; Zan, R.; Shen, Z.; Wang, C.; Peng, P.; Wang, J.; Sun, B.; Xiao, B.; Li, Q.; Liu, S.; et al. Remarkable bioactivity, bio-tribological, antibacterial, and anti-corrosion properties in a Ti-6Al-4V-xCu alloy by laser powder bed fusion for superior biomedical implant applications. *Chem. Eng. J.* **2023**, *471*, 144656. [CrossRef]
14. Chen, Y.; Yang, W.; Zhu, S.; Shi, Y. Microstructural, mechanical and in vitro biological properties of Ti_6Al_4V-5Cu alloy fabricated by selective laser melting. *Mater. Charact.* **2023**, *200*, 112858. [CrossRef]

15. Li, Y.; Luo, W.; Liu, Y.; Lu, Y.; Geng, W.; Lin, J. Copper-containing titanium alloys promote the coupling of osteogenesis and angiogenesis by releasing copper ions. *Biochem. Biophys. Res. Commun.* **2023**, *681*, 157–164. [CrossRef]
16. Akbarpour, M.R.; Mirabad, H.M.; Hemmati, A.; Kim, H.S. Processing and microstructure of Ti-Cu binary alloys: A comprehensive review. *Prog. Mater. Sci.* **2022**, *127*, 100933. [CrossRef]
17. Cardoso, F.F.; Cremasco, A.; Contieri, R.J.; Lopes, E.S.N.; Afonso, C.R.M.; Caram, R. Hexagonal martensite decomposition and phase precipitation in Ti–Cu alloys. *Mater. Des.* **2011**, *32*, 4608–4613. [CrossRef]
18. Zhang, D.; Qiu, D.; Gibson, M.A.; Zheng, Y.; Fraser, H.L.; StJohn, D.H.; Easton, M.A. Additive manufacturing of ultrafine-grained high-strength titanium alloys. *Nature* **2019**, *576*, 91–95. [CrossRef]
19. Zhang, L.C.; Klemm, D.; Eckert, J.; Hao, Y.L.; Sercombe, T.B. Manufacture by selective laser melting and mechanical behavior of a biomedical Ti–24Nb–4Zr–8Sn alloy. *Scr. Mater.* **2011**, *65*, 21–24. [CrossRef]
20. Thijs, L.; Kempen, K.; Kruth, J.-P.; Van Humbeeck, J. Fine-structured aluminium products with controllable texture by selective laser melting of pre-alloyed AlSi10Mg powder. *Acta Mater.* **2013**, *61*, 1809–1819. [CrossRef]
21. Fischer, M.; Joguet, D.; Robin, G.; Peltier, L.; Laheurte, P. In situ elaboration of a binary Ti–26Nb alloy by selective laser melting of elemental titanium and niobium mixed powders. *Mater. Sci. Eng. C* **2016**, *62*, 852–859. [CrossRef] [PubMed]
22. Attar, H.; Calin, M.; Zhang, L.C.; Scudino, S.; Eckert, J. Manufacture by selective laser melting and mechanical behavior of commercially pure titanium. *Mater. Sci. Eng. A* **2014**, *593*, 170–177. [CrossRef]
23. Yi, C.; Ke, Z.; Zhang, L.; Tan, J.; Jiang, Y.; He, Z. Antibacterial Ti-Cu alloy with enhanced mechanical properties as implant applications. *Mater. Res. Express* **2020**, *7*, 105404. [CrossRef]
24. Brodie, E.G.; Medvedev, A.E.; Frith, J.E.; Dargusch, M.S.; Fraser, H.L.; Molotnikov, A. Remelt processing and microstructure of selective laser melted Ti25Ta. *J. Alloys Compd.* **2020**, *820*, 153082. [CrossRef]
25. Polozov, I.; Sufiiarov, V.; Kantyukov, A.; Popovich, A. Selective Laser Melting of Ti_2AlNb-based intermetallic alloy using elemental powders: Effect of process parameters and post-treatment on microstructure, composition, and properties. *Intermetallics* **2019**, *112*, 106554. [CrossRef]
26. *ASTM B962-23*; Standard Test Methods for Density of Compacted or Sintered Powder Metallurgy (PM) Products Using Archimedes' Principle—Annual Book or ASTM Standards, Vol. 2.5. American Society for Testing and Materials: West Conshohocken, PA, USA, 2023.
27. *ASTM E 8M*; Standard Test Methods of Tension Testing of Metallic Materials [Metric]—Annual Book or ASTM Standards, Vol. 3.01. American Society for Testing and Materials: West Conshohocken, PA, USA, 2022.
28. Taguchi, O.; Iijima, Y. Diffusion of copper, silver and gold in α-titanium. *Philos. Mag. A* **1995**, *72*, 1649–1655. [CrossRef]
29. Thijs, L.; Verhaeghe, F.; Craeghs, T.; Van Humbeeck, J.; Kruth, J.-P. A study of the microstructural evolution during selective laser melting of Ti–6Al–4V. *Acta Mater.* **2010**, *58*, 3303–3312. [CrossRef]
30. Zhou, Y.L.; Niinomi, M.; Akahori, T.; Nakai, M.; Fukui, H. Comparison of Various Properties between Titanium-Tantalum Alloy and Pure Titanium for Biomedical Applications. *Mater. Trans.* **2007**, *48*, 380–384. [CrossRef]
31. Liu, J.; Chang, L.; Liu, H.; Li, Y.; Yang, H.; Ruan, J. Microstructure, mechanical behavior and biocompatibility of powder metallurgy Nb-Ti-Ta alloys as biomedical material. *Mater. Sci. Eng. C* **2017**, *71*, 512–519. [CrossRef]
32. Zhenhuan, W.; Yu, D.; Junsi, L.; Xiaowei, J.; Zongyu, X.; Li, L.; Xiaoli, X. Physiochemical and biological evaluation of SLM-manufactured Ti-10Ta-2Nb-2Zr alloy for biomedical implant applications. *Biomed. Mater.* **2020**, *15*, 045017. [CrossRef]
33. Kasperovich, G.; Hausmann, J. Improvement of fatigue resistance and ductility of TiAl6V4 processed by selective laser melting. *J. Mater. Process. Technol.* **2015**, *220*, 202–214. [CrossRef]
34. Ackers, M.A.; Messé, O.M.D.M.; Manninen, N.; Stryzhyboroda, O.; Hecht, U. Additive manufacturing of TTFNZ (Ti-4.5Ta-4Fe-7.5Nb-6Zr), a novel metastable β-titanium alloy for advanced engineering applications. *J. Alloys Compd.* **2022**, *920*, 165899. [CrossRef]
35. Gong, H.; Rafi, K.; Gu, H.; Starr, T.; Stucker, B. Analysis of defect generation in Ti–6Al–4V parts made using powder bed fusion additive manufacturing processes. *Addit. Manuf.* **2014**, *1*, 87–98. [CrossRef]
36. Sinha, A.; Swain, B.; Behera, A.; Mallick, P.; Samal, S.K.; Vishwanatha, H.M.; Behera, A. A Review on the Processing of Aero-Turbine Blade Using 3D Print Techniques. *J. Manuf. Mater. Process.* **2022**, *6*, 16. [CrossRef]
37. Niinomi, M.; Nakai, M.; Hieda, J. Development of new metallic alloys for biomedical applications. *Acta Biomater.* **2012**, *8*, 3888–3903. [CrossRef]
38. Liu, R.; Memarzadeh, K.; Chang, B.; Zhang, Y.; Ma, Z.; Allaker, R.P.; Ren, L.; Yang, K. Antibacterial effect of copper-bearing titanium alloy (Ti-Cu) against *Streptococcus mutans* and *Porphyromonas gingivalis*. *Sci. Rep.* **2016**, *6*, 29985. [CrossRef]
39. Sing, S.L.; Yeong, W.Y.; Wiria, F.E.; Tay, B.Y. Characterization of Titanium Lattice Structures Fabricated by Selective Laser Melting Using an Adapted Compressive Test Method. *Exp. Mech.* **2016**, *56*, 735–748. [CrossRef]